http://dx.doi.org/10.1016/j.jobe.2023.108175


# Spray parameter analysis and performance optimization of indirect evaporative cooler considering surface wettability

Xiaochen Ma [a,*], Wenchao Shi [a], Hongxing Yang [a,**]

[a] Renewable Energy Research Group (RERG), Department of Building Environment and Energy Engineering, The Hong Kong Polytechnic University, Hong Kong, China

## Abstract

Along with the increasing energy consumption of space cooling, the building industry is in urgent need of the environmental-friendly and proven cooling technology. Indirect evaporative cooling (IEC) is attracting wider attention as a sustainable technology based on the heat absorption properties of evaporation. It has been demonstrated that the plate surface covered by the water membrane in the wet channels has a substantial effect on the operating performance in the practical use of IEC technology, while the ideal state of the uniform water distribution assumed by existing models is usually difficult to be achieved. In order to enhance the evaporation process, it is crucial to tune the nozzle features in water supply session and organize the nozzles suitably over the heat exchanger. In this study, a three-dimensions Computational Fluid Dynamics (CFD) model is therefore proposed, which considers the actual wetting factor of the plate surface. In addition, the movement of the spray droplets as well as the formation and flow state of the water film covering the plate surface, are reflected in the simulation model to predict the performance of the IEC under normal operation more accurately. The results depicted that the maximum coverage area could be achieved when the diameter of the spray droplet maintains 0.25 mm with the flow rate is 5.4 L/min, and the distance between two nozzles is 80 mm. Besides, the maximum value of the wet-bulb efficiency and the coefficient of performance (COP) of the IEC system with optimized nozzle parameter settings could be improved up to 15.1% and 17.6% respectively compared to the conventional one. The proposed 3D model could contribute to the improvement of further IEC technique by providing a homogeneity of the water film covered on the plate surface to reflect future research into the heat and mass transfer mechanisms of hydrophilic materials.

**Keywords**: Indirect evaporative cooler, Wettability, CFD model, Nozzle settings, Optimization

* Corresponding author.
** Corresponding author.
*E-mail addresses*: xiaochencc.ma@connect.polyu.hk (X. Ma), hong-xing.yang@polyu.edu.hk (H. Yang).

**Nomenclature**

| | | | |
|---|---|---|---|
| *IEC* | Indirect evaporative cooling | $Re_s$ | Reynolds number |
| *CFD* | Computational Fluid Dynamics | $d_e$ | the diameter of the channel, m |
| *DPM* | Discrete Phase Model | $f_{Re}$ | friction coefficient |
| *EWF* | Eulerian Wall Film Model | *Dd* | droplet diameter |
| *COP* | coefficient of performance | *Fr* | flow rate |
| *Symbols* | | *Greek letters* | |
| *H* | distance of the nozzle position, mm | $\varphi$ | coverage ratio |
| *Q* | water flow rate, kg/s | α | the volume fraction of the stage |
| *P* | pressure, Pa | $\varepsilon_{wb}$ | wet-bulb efficiency |
| $\mu$ | dynamic viscosity, kg/(m·s) | | |
| *u* | velocity, m/s | *Subscripts* | |
| *v* | kinetic velocity, m/s | *p* | the primary air |
| $\overline{\omega}$ | longitudinal velocity, m/s | *s* | the secondary air |
| $\delta_w$ | the thickness of the water membrane, mm | *w* | water section |
| $\sigma$ | wetting factor | *in* | airflow at the inlet |
| $C_D$ | drag coefficient | *out* | airflow at the outlet |
| $u_l$ | water film velocity, m/s | *pl* | the plate surface area |
| ρ | density, kg/m$^3$ | *k* | thermal conductivity, (W/(m·K)) |
| *RH* | relative humidity | *g* | gravitational acceleration, (m/s$^2$) |
| *W* | power, kW | | |

## 1 Introduction

With the drastic changes in the climate and the higher standards for indoor air quality, the total energy consumption required to maintain the building environment has increased significantly, occupied for about 26.9% of global energy usage [1,2]. As for Hong Kong, space cooling is responsible for over 50% of the whole energy consumed in construction, especially for public buildings with high fresh air demands [3]. The 'Energy Saving Plan (2015 – 2025)' unveiled by the Environment Bureau of the Hong Kong SAR Government aims at reducing 40% energy intensity by 2025 [4]. Therefore, in order to reduce the demand for electricity power, it is crucial to strongly promote sustainable cooling technologies. The indirect evaporative cooler (IEC) uses less energy with less greenhouse gas production by exploiting the latent heat of water evaporation, which has attracted the interest of numerous relevant researchers [5,6].

By making full utilization of latent heat from water evaporation, the IEC system is expected to significantly reduce the peak load of mechanical plants and save 17% to 35% on the electricity consumption of fresh air handling [7,8]. The IEC unit always contains an amount of dry and wet channels that are split by plates of the heat exchanger and is motivated by a submersible pump and two fans [9]. The primary air travelling through the dry channels would be sensibly cooled without humidity added when water is supplied into the wet channels, reducing bacterial growing and enhancing thermal comfort [10]. As a common cooling equipment with substantial highlights, the primary affecting elements of the operational ability of the IEC device have been gradually elucidated in the previous study, especially the heat-mass transition that occurred in the course of the operation period of the heat exchanger [11]. The evaporation phenomenon in wet channels has been regarded as one of the most critical thermodynamic aspects of IEC, which reduces the surface temperature of the heat exchanger and transfers a substantial amount of heat from the dry to the wet side [12]. Typically, a higher water evaporation efficiency will be used to accomplish better cooling efficiency of the coolers [13].

Numerous studies on the composition and design of the channel plate have been done in an effort to improve the evaporation process that occurs in wet channels. The wet-bulb efficiency was analysed by Antonellis et al. through an experimental research of an IEC manufactured from five different geometries of heat exchangers with different plate protrusions and spacing as variables. It was finally concluded that the mesh plate protrusions had optimal heat transfer performance while ensuring plate stiffness [14]. Guilizzoni et al. [15] then analysed two IEC systems with different plate coatings in combination with different water distribution systems and inferred that the contact angle of the hydrophilic paint was always less than that of the epoxy coating and that there was a 10% improvement in the wet-bulb efficiency of the IEC when applied in combination with the TOP water distribution solution. You et al. [16] conducted experimental research on two different hydrophilic material coatings for IEC systems, and the IEC with hydrophilic coatings showed improvement in wet-bulb efficiency and COP. Chen et al. [17] demonstrated through experimental studies that plant fibre polymer composites, which are inexpensive and lightweight, are promising for IEC applications, improving the wettability and enhancing the cooling capacity of IEC. Shi et al. [18] propose the porous material applied as the heat transfer plate, which could save water on the plate to support intermittent water spray, and maintain wettability for a longer time with power reduced. He also proved that the COP raised by an mean value of 117.5% in comparison with the conventional continuous water supply mode [19]. However, the disadvantage of high workload and relatively high expense is present in almost all of these systems.

Furthermore, another direction worth focusing on is the arrangement parameter of spray nozzles. Through studies, Sun et al. [20] experimentally tested five different types of commonly used nozzles

and found that spiral nozzles provided the highest coverage and the best uniformity. However, the cooling capacity of the IEC system only increased in a specific range with increasing water spray flow. Antonellis et al. [21] studied the five different configurations of water nozzles over IEC and determined that the TOP configuration consumed the least amount of water while maintaining the highest wet bulb efficiency. It was found that a better spray configuration resulted in more surface contact region and reduced the heat transfer resistance between the two air flows. Cristina et al. used CFD simulations to optimize the nozzle characteristics of a double-layer façade (DSF) for dry thermal conditions with evaporative cooling. The study determined that the optimal DSF configuration comprises an air cavity width of 0.4 m, droplets of 25 μm, and a nozzle spacing of 0.6 m [22]. Besides, a comprehensive study of the performance of optimised nozzle arrangements on IEC using a mathematical model developed by Ma et al. [23] found that optimised arrangements could lead to a 16% increase in wet-bulb efficiency.

In addition, the water droplet sprayed distribution above the secondary air channel is mostly assumed as the steady water membrane evenly covering the heat exchanger surface in the previously proposed numerical models of IEC. Kettleborough and Hsieh [24] firstly opposed a heat and mass transfer model for an IEC by assuming the uniform film wettability throughout the wet surface plastic plates. A simple wettability factor $\sigma$ that varied from 0 to 1 was firstly used to explain the impact of incomplete wetting characteristics Later, Ren and Yang [25] selected a grouped parameter $\sigma/Le_f$ varying from 0.5 to 1.1 in an effectiveness-NTU model of IEC to discuss the impact of surface wettability on cooling capacity. Cui et al. [26] proposed a mathematical model of IEC with an assumed water film thickness ranging from 0.2 to 0.5 mm. The thermal resistance for conduction in water membrane was negligible as calculated below $8.5\times10^{-4}$ $m^2 \cdot K/W$. De Antonellis et al. [27] correlated the surface wettability factor in an IEC model to the working air and water flow rate. By assuming no water droplets in the air stream, an enhancement in the spray flow rate generally led to a linear growth of the $\sigma$. Few studies have considered the uniformly wetted conditions on the plate surface with variable water mass flow rates at the cross-section.

A complete IEC system, however, encounters numerous issues in realistic operation, which could result in serious water evaporation issues, like: 1) the distributed water droplets with an inappropriate diameter will be in a state of drift, so that the sprayed droplets are moved out with the departing air flow without enough evaporation; 2) the coverage region of water film occupied the plate surface would be poor since the high surface tension of water and unsuitable nozzle parameter settings.

Due to the impact of surface wettability on IEC cooling potential has been the core of the numerical studies, and the actual wetting conditions are rarely expressible in terms of a single, constant value of surface wettability. For IECs, there is still a dearth of compelling and comprehensive mathematical models covering water supply systems so as to synthesise the water droplet spraying and the thin water membrane generation on the channel surface of the water supply system. Therefore, a spray model on the basis of Computational Fluid Dynamics (CFD) will be developed for IEC in this paper, enabling the simulation of dynamic process of water droplets produced from the nozzles and entrained in water film along the surface. A test bench with a complete IEC system was set up to investigate the practical wetted sections on the surface of one channel pair for model verification. Validated by the experimental consequences, the developed numerical model could be applied to further parametric analysis and optimization on IEC performance. The optimal design on influencing parameters could be obtained by a series of simulation work. To further understand the current research, a flow chart is demonstrated in Fig. 1.

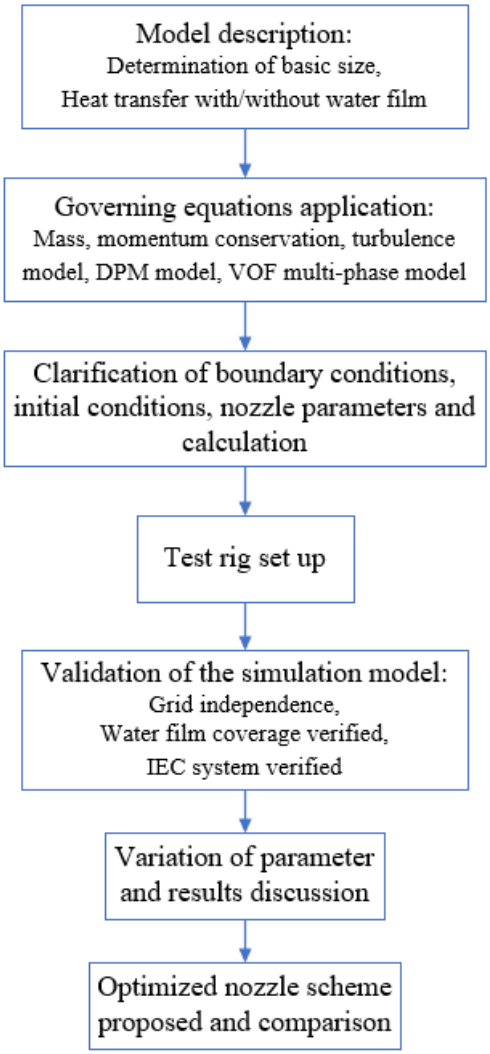


Fig.1. Flowchart for this research

## 2 Model description

### *2.1 Model geometry*

The baseline model will be presented through Space claim in ANSYS workbench, where the water film coverage coefficient of the wet channel plate surface is specifically set up and used as a key research factor in this study. A set of hypotheses are presented below for in-depth study.

- The characteristics of the fluids are constant and the entire fluid is incompressible.
- The plate of the heat exchanger is adiabatic, so radiation heat transfer is ignored.
- The water film covering the wet channel is not uniform and completely covered, but its thickness is thin due to the fluidity of the film and the amount of water.

A complete IEC system usually consists of three parts: 1) heat exchanger with alternative dry and wet channels, 2) water spray system, and 3) two separate air loops. On account of the similarity of heat and mass transfer generated within the same type of channel, the two-channel (dry and wet channel) heat exchanger model will be considered here as a representative object of study, as depicted in Fig. 2. A solid conical nozzle is provided at a height of above the heat exchanger keeps the water flow in the wet channel and the secondary airflow in a reverse direction. The water system works by releasing a series of water droplets from the nozzles, some of which get into touch with the flat plate and produce a water film that runs down the plane. At the same time, secondary airflow flows from

the bottom to the top of the wet channel, where it comes into contact with the downward flowing liquid film.

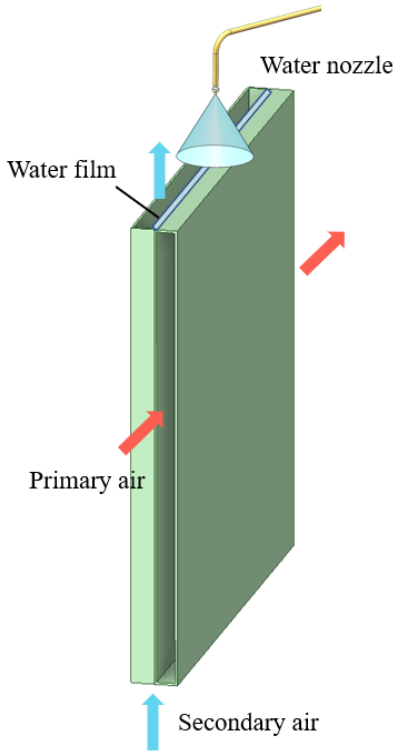


Fig. 2. Configuration of an IEC system with single channel

By virtue of the spread features of water, the water film formed by spraying often does not allow the plate surface of the wet channel to be completely wet, and the study conducted by Yang et al [28], confirmed that there is a clear difference in heat and mass transfer at the wet and dry sections of the wet channel as identified in Fig. 3.

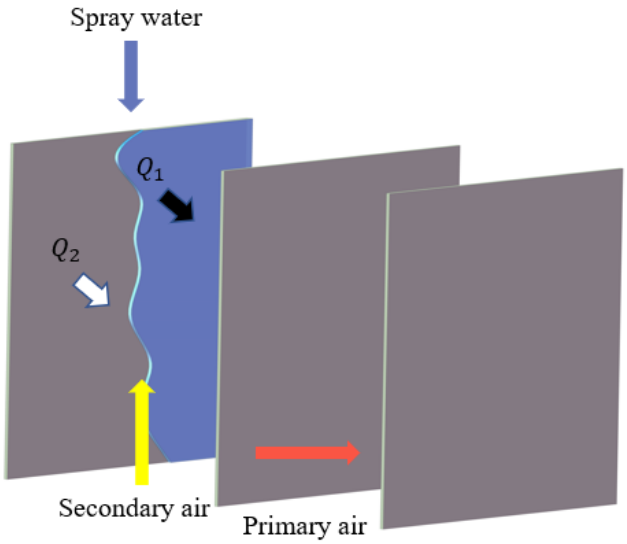


Fig. 3. Demonstration model of a single channel pair of a plate cross-flow IEC

Therefore, a coverage factor—defined as a proportion of the wetted section assigned on the entire plate surface, as stated by Eq. (1) [28]—should be introduced to evaluate the performance of the water film distribution.

$$\varphi = \frac{A_w}{A_{pl}} \tag{1}$$

where $\varphi$ represents the coverage factor of the plate surface; $A_w$ represents wet section for water membrane evaporation; $A_{pl}$ represents the entire plate surface area.

*2.2 Control equations*

In contrast to previous approaches to modelling IEC fluids, this study combines the nozzle spray process with the water droplet contact and formation of water film process based on heat and mass exchange between air flows. Therefore, the model of the nozzle spray, water film formation and heat exchanger should be considered comprehensively. The specific formulations for the control principles are as follows:

(1) Conservation of momentum transfer

$$\frac{\partial}{\partial \mathrm{t}}(\rho \mathrm{E}) + \nabla \cdot (\rho \mathrm{u}^2) = -\nabla \mathrm{P} + \nabla \cdot \left(\mu(\nabla \mathrm{u} + \nabla \mathrm{u}^{\mathrm{T}})\right) + \rho \mathrm{g} + \mathrm{F} \tag{2}$$

(2) Conservation of mass

$$\frac{\partial}{\partial \mathrm{t}}(\rho) + \nabla \cdot (\rho \mathrm{u}) = 0 \tag{3}$$

(3) Conservation of energy

$$\nabla \cdot \sum_{k=1}^{n} \left(\alpha_k v_k \left(\rho_k E_k + p\right)\right) = \nabla \cdot (k_{eff} \nabla T) + S_E \tag{4}$$

(4) VOF multi-phase model

Due to the presence of both air and water flow in the IEC system during operation and the fact that the liquid has both drop and film forms, the multi-phase flow model needs to be applied here. Each numerical grid in the VOF model has a density and viscosity that were represented by Eqs. (5), (6), (7).

$$\rho = \alpha_1 \rho_1 + \alpha_g + \rho_g \tag{5}$$

$$\mu = \alpha_1 \mu_1 + \alpha_g + \mu_g \tag{6}$$

$$\frac{\partial \alpha_{1/g}}{\partial t} + \vec{u} \cdot \nabla \alpha_{1/g} = 0 \tag{7}$$

(5) Discrete phase (spray droplets) model

In this study, the DPM model was used to complete the nozzle spray conditions above the heat exchanger, taking into consideration random collisions, coalescence and break-up. The discrete phase droplets will therefore be subject to inertia, the gas phase aerodynamic drag force, as well as gravity. By resolving the force balance equation represented by Eq. (8), the track of the droplets could be calculated using a joint Euler-Lagrangian approach.

$$\frac{d\left(\overrightarrow{X_g}\right)}{dt} = \overrightarrow{V_g} \tag{8}$$

where $\vec{V}_g$ is the speed of droplet (m/s); and $\vec{X}_g$ is the location of droplet (m).

The second law proposed by Newton is applied here to predict the speed of evaporating circular particles of water moving in a steady flow. Air and droplet connection via two methods facilitate the exchange of mass and heat with air. Eq. (9), a mathematical formula, describes how a single droplet moves.

$$\frac{d\left(m_d\overrightarrow{F_d}\right)}{dt} = \overrightarrow{F_D} + \overrightarrow{F_g} \tag{9}$$

The drag power performs in the direction contrary to the comparable speed of the moving droplet towards the airflow. The size and shape of the water droplet, its comparable speed to the airflow, and the property of the air all affect the force generated [29]. All these influencing factors are taken into account by the drag coefficient. The drag force could be described as Eq. (10).

$$\vec{F}_d = -\frac{\pi}{8} C_D \rho_a D_d^2 \vec{V}_r \left|\vec{V}_r\right| \tag{10}$$

where $C_D$ is the drag factor, $\vec{V}_r$ represents the relative speed of droplet ($m \cdot s^{-1}$).

(6) Eulerian Wall Film (EWF) model

The formation and flow of the water membrane covered along the plate surface should be considered so as to properly characterize the physical processes occurring inside the IEC wet channel. The water droplet injected by the nozzle then trapped by the plate could be seen as transfer to the water membrane and flow down along the wall surface, following the association as Eq. (11) and Eq. (12).

$$\frac{\partial \delta}{\partial t} + \nabla \cdot (\delta u_l) = \frac{\dot{m}_s}{\rho_l} \tag{11}$$

$$\dot{m}_s = \alpha_l \rho_l u_{l,n} \tag{12}$$

(7) Species transport model

The phase change process causes some heat mass movement in the wet channel of the IEC by virtue of evaporation, hence the simulation must include the species transfer model developed by Eq. (13) in order to properly account for this.

$$\frac{\partial C_i}{\partial t} + \nabla J_i = R_i \tag{13}$$

*2.3 Boundary conditions*

The modelling of the overall IEC system relies on the application of the commercial CFD software Fluent, where the heat combined mass transfer between fluids and the evaporation procedure of the water membrane is considered while the spray is simulated to eject and contact with the heat exchanger plate to produce the continuous water membrane, thus the overall boundary status is explicitly represented as follows.

For the dry channel, the front side is used as the air inlet for the primary airflow while the back side is used as the air outlet in contrast. For the secondary air channel, the bottom side of the heat exchanger is defined as the secondary air entrance and the top side as the air outlet. In addition, based on previous assumptions, all panels included in the heat exchanger are set up as adiabatic walls. For the water film section, the inner plate of the wet channel is considered as an absorbable wall for the DPM model with Eulerian liquid film transformation and coupling under certain conditions. The structured grid is applied and the meshing mode used in this model is depicted in Fig. 4. Besides, the water membrane had such a thin film thickness across the heat exchanger plate during the simulation

time, so the flow characteristics of the film were captured using a finite mesh with dimensions not exceeding 0.1 mm for the region nearby the wall.

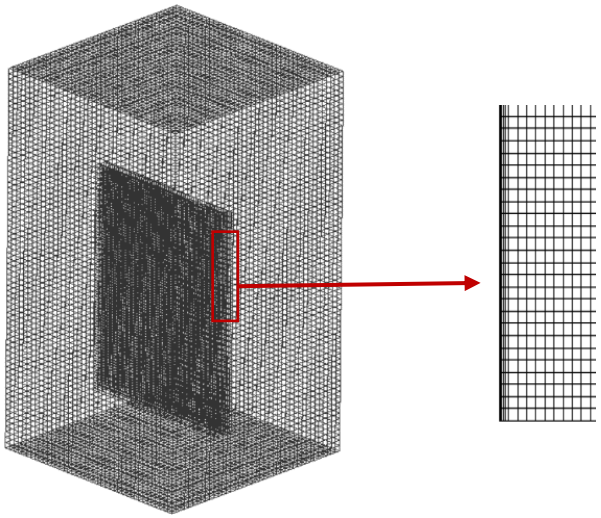

Fig. 4. Sketches for the division of the numerical model into meshes

*2.4 Performance indexes*

*2.4.1 Performance of water membrane distribution*

This research applied coverage ratio as the assessment index to assess the effectiveness of water distribution situation written from Eq. (1), which has been mentioned in section 2.1.

$$\varphi = \frac{A_w}{A_{pl}} \tag{1}$$

*2.4.2 Performance of IEC operation*

The wet-bulb efficiency would be utilized as a constructive metric to estimate the entire working ability of the IEC system. It is often applied to delineate the extend that the primary air outflow temperature close to the wet-bulb temperature of the secondary air inlet [30], depicted as Eq. (14).

$$\varepsilon_{wb} = \frac{t_{p,in} - t_{p,out}}{t_{p,in} - t_{wb,s}} \tag{14}$$

Another effective metric for assessing the performance of an IEC is energy usage. The overall energy expenditure of a complete IEC system is far lower than that of a mechanical air-conditioning system since, being a green technology, it only uses the power necessary to support the normally running of the circulation water pumps as well as the airflow fans. The following equation could be used to estimate IEC energy consumption according to some fundamental definitions and descriptions of terms as well as coefficient values utilizing empirical equations referring to Min et al. [31].

By using a hydraulic calculation method to determine the pressure drop, it is possible to compute the power need of each fan:

$$f_{Re} = 96 * (1 - 1.3553(\frac{L}{s}) + 1.9467\left(\frac{L}{s}\right)^2 - 1.7012\left(\frac{L}{s}\right)^3 + 0.9564\left(\frac{L}{s}\right)^4 - 0.2537\left(\frac{L}{s}\right)^5) \tag{15}$$

$$d_e = \frac{2sL}{s + L} \tag{16}$$

$$\triangle P = \frac{f_{Re} L \rho u^2}{2Red_e} \tag{17}$$

Thus, the energy consumption caused by the fans is described like:

$$W_{fan} = \frac{Q \triangle P}{3600 \times 1000 \times \eta_0 \times \eta_1} \times K \tag{18}$$

The following equation is employed to figure out the energy consumption of water pump:

$$W_{pump} = m_w g\left(h_{gravity} + h_{nozzles} + h_{valves}\right) \times K \tag{19}$$

The COP value can be used in this study to gauge how energy-efficiently refrigeration operates for various nozzle setting schemes [32], and the determined formula is:

$$Q_p = m_p c_{pg}\left(t_{p,in} - t_{p,out}\right) \tag{20}$$

$$COP = \frac{Q_p}{W_{fan} + W_{pump}} \tag{21}$$

## 3 Experiment and verification

### *3.1 Description of experimental system*

A test bench was set up as depicted in Fig. 5 so as to verify the proposed simulation model. The three core components of the experimental system were a plate heat exchanger, a water supply equipment, and an air supply device, respectively. As an essential part of the IEC, the heat exchanger, which is built up of alternate dry and wet channels. Each aluminium plate that makes up the heat exchanger is the same size, 0.25 m × 0.4 m × 0.4 m, with the surface of each plate showing microscopic protrusions inwards and outwards, as well as every two aluminium plates meeting head to tail to form a 4 mm channel gap to support the flow of air through. When the experimental system is in normal operation, a fan set at the bottom of the heat exchanger supplies a continuous stream of dry secondary air upwards. At the same time, a nozzle built above supplied water into the heat exchanger in a counterflow configuration to the secondary airflow. During this process, some of the water droplets that are sprayed in the heat exchanger come into contact with the heat exchanger walls and form a water membrane that slides down the walls. With the purpose of allowing the spread of the water film covered on heat exchanger plates to be observed, a transparent panel of plastic is provided on the outermost side. In addition, the nozzles on top of the system will be mounted on slides so that the nozzles can be moved to different distances from the observable walls to support the validation work.

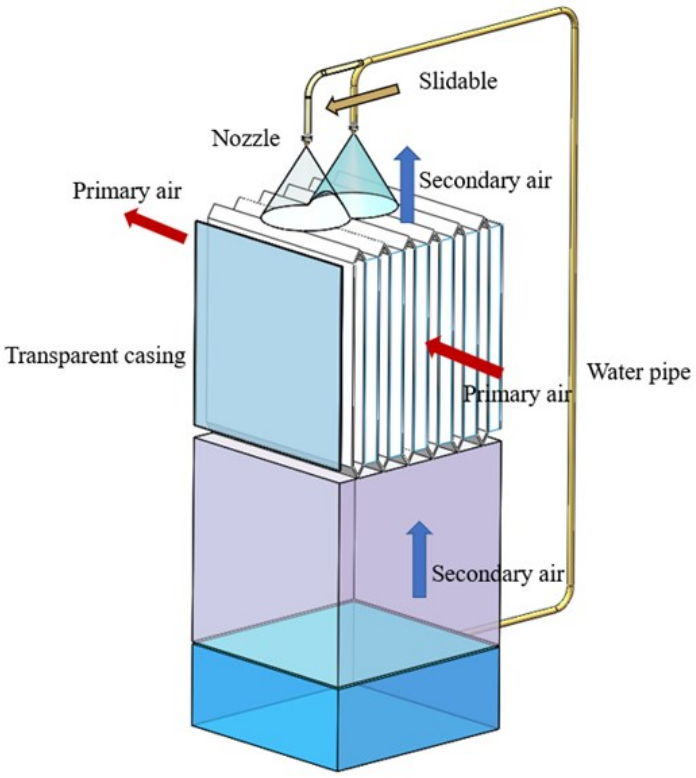


Fig. 5. The test bench for the IEC water spray system

### *3.2 Model Validation*

#### *3.2.1 The proof of grid independence*

The mesh computational model was subjected to the ICEM software in ANSYS work bench. In general, the precision of the calculation increases with the quality of the grid, but the time taken increases when the number of grids is too large. The compromise between computational precision and time consumption is therefore critical and the most appropriate number of meshes needs to be determined so as to keep the precision of the consequences within reasonable limits while reducing computational time.

In Fig. 6, the coverage ratio calculated by the model at different numbers of grids is shown separately. It is evident that the calculated value clearly increases with the number of grids and then plateaus at grid number of 113,200, which is therefore determined as the grid count for subsequent simulations.

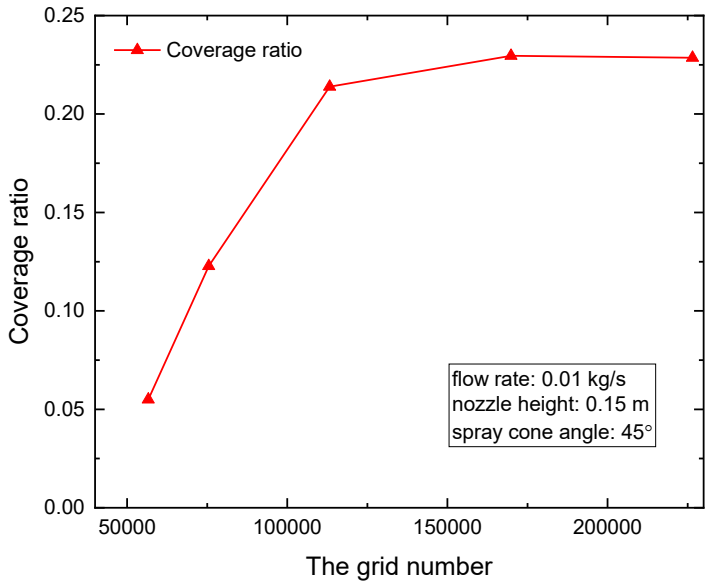


Fig. 6. Coverage factor at different accounts of grid

### *3.2.2 Water film coverage validation*

In terms of coverage area occupied by water film, the suggested CFD-based water membrane distribution model was validated. The divided grid will be provided to help collect the water film covering area on the surface of plate. Fig. 7 (a) and (b) individually show the division sample of the genuine experimental and simulation modes. On this basis, ImageJ software was applied to specify the area of the heat exchanger plate covered by the water film (Fig. 7 (c)). The specific steps are to adjust the scale of the picture, then set the picture properties to grey scale display, and finally the contour of the wetted part is indicated by a line to obtain the accurate coverage area.

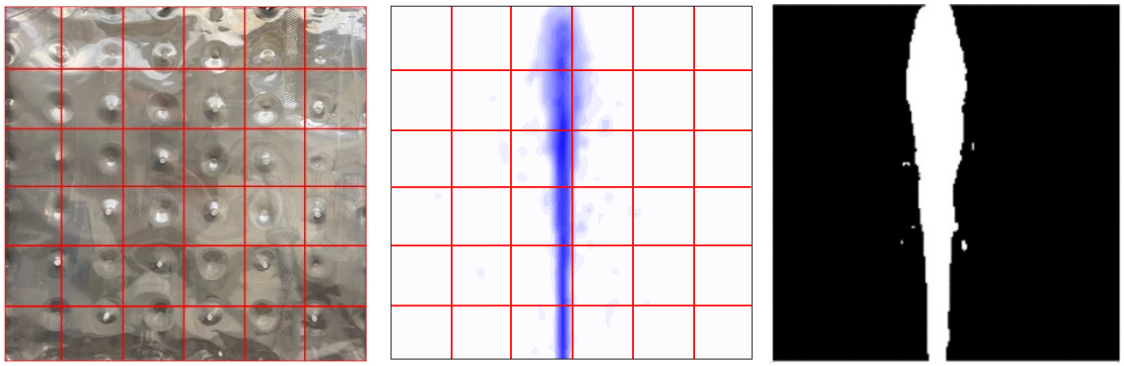

(a) Experiment mode (b) Numerical mode (c) Experiment mode in ImageJ

Fig. 7. Demonstration of the division sample

Besides, the water circulation in this experiment was primarily powered by a pump system located in the water reservoir. A flowmeter and a manometer are set up as measuring instruments on the section of the water pipe from the pump to the nozzle, respectively. The bracket limits the spray height to 0.15 m, and the frequency converter pump combined with a valve regulates the water flow in the pipe. Fig. 8 depicts the photos of instruments, and Table 1 has a description of the feature of each tool.


(a) Flowmeter (b) Pressure gage

Fig. 8. Photos of the test instruments

Table 1 Specifications of the instrument

| Instrument | Parameter | Range | Accuracy |
|---|---|---|---|
| Flow meter | Flow rate of water | 0-0.1 L/h | ±1% |
| Manometer | Pressure | 0-1500 kPa | ±1% |

Uncertainty analysis of the data from the test results is essential due to the errors introduced by the accuracy of the measurement equipment during the experiment [33,34]. Eqs. (22), (23) provide methods on how to figure out the uncertainty of measurement models and experimental parameters, separately.

$$U = f(x_1, x_2, x_3, \dots, x_n) \tag{22}$$

$$\delta U = \sqrt{\left(\frac{\delta U}{\delta x_1}\delta x_1\right)^2 + \left(\frac{\delta U}{\delta x_2}\delta x_2\right)^2 + \left(\frac{\delta U}{\delta x_3}\delta x_3\right)^2 + \cdots + \left(\frac{\delta U}{\delta x_n}\delta x_n\right)^2} \tag{23}$$

where $\delta U$ represents the entire uncertainty of the specified parameter, and $\delta x_n$ is the uncertainty of each measurement $x_n$. Based on the precision data of per measurement apparatus listed in Table 1, the error of the coverage factor by the trial evaluation standard is 2.31%.

The simulation model also made use of the original experimental test settings, which are carried out on the basis of the subsequent conditions: $Q$ = 0.01 kg/s, $\alpha$ = 45°, and $H$ = 0.15 m. Fig. 9 reflects the simulation results for coverage compared to the experimental results and finds that these points lie within 20% of the deviation and that the maximum difference is 7.1%, which is acceptable for subsequent studies.

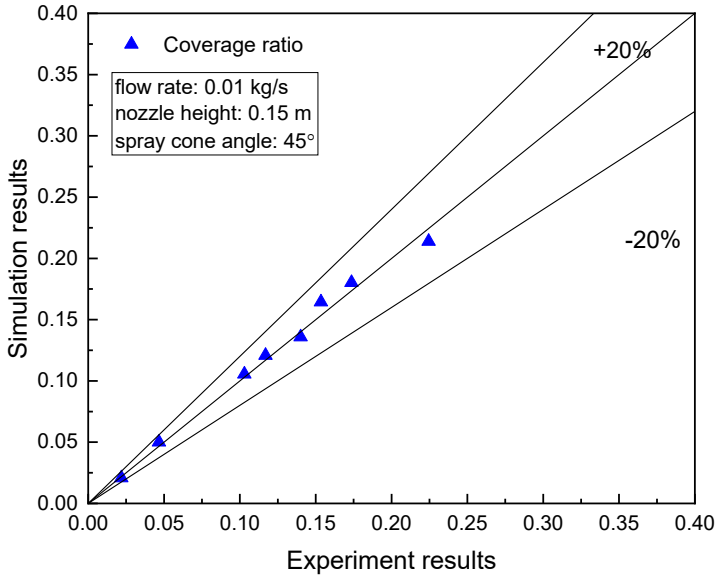


Fig. 9. Comparison between the experiment and simulation results

*3.2.3 IEC system validation*

To combine the water film coverage area with the performance of the whole IEC system, another more complete model with validation experiment should be carried out. On the foundation of section 3.2.1, the ICEM program in ANSYS was still used to build a numerical model of the mesh, taking into account the temperature and humidity factors with heat and mass convey. Fig. 10 described the test rig of a complete IEC system, which consist primary air channel, secondary air channel as well as water spray system, and the fixed parameters of experimental setting were shown in Table 2. The entire setup was done in a lab with regulated humidity and temperature levels. Table 3 lists the test conditions and the details of the measurement equipment. A data logger recorded, showed, and recorded every piece of tested data, at 2-second intervals.

Table 2 Setpoint of the IEC for simulation

| Parameter | Value | Units |
|---|---|---|
| Channel number | 25 | - |
| Channel gap | 4 | mm |
| The length of IEC | 250 | mm |
| No. of nozzles | 2 | - |

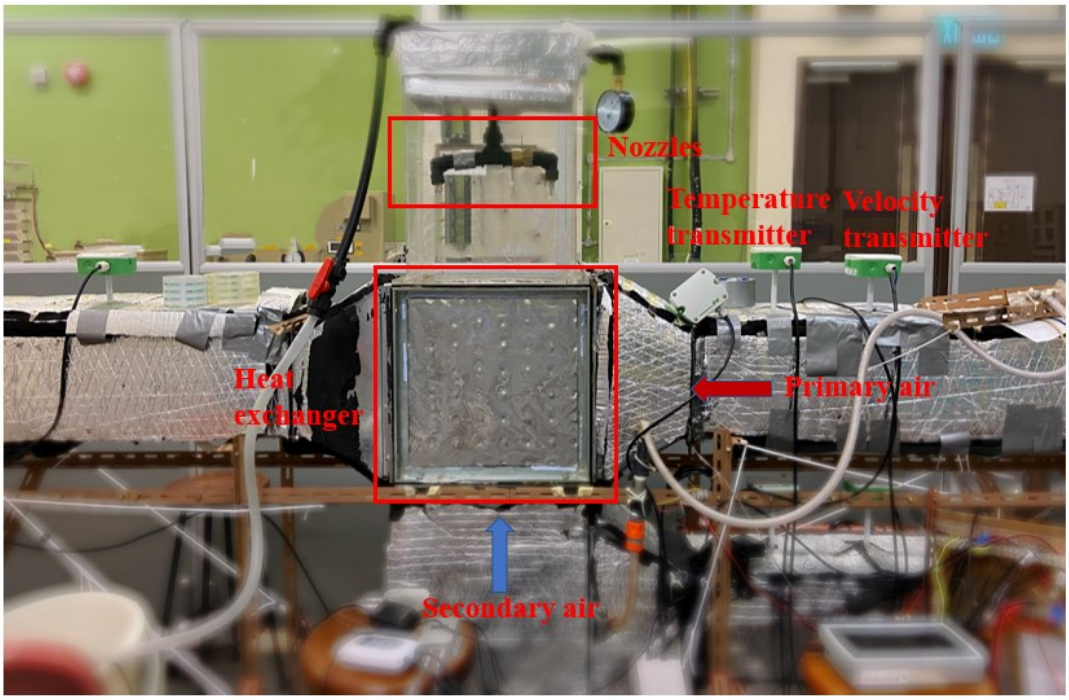


Fig. 10. The test bench for the complete IEC system

Table 3 Specifications of the test values

| Instrument | Value | Range | Accuracy |
|---|---|---|---|
| Temperature | Temperature sensor EE160 | -10-60 ℃ | ± 0.2% ℃ |
| Relative humidity | Humidity sensor EE160 | -15-95% RH | ±2% RH |
| Air speed | Velocity sensor EE65 | 0-0.17 m/min | ±2% |

According to Table 3 and Eqs. (22), (23), the results of uncertainty analyses could be determined. Based on the precision statistics for each measuring device indicated in Table 3, the error of the wet-bulb efficiency by the test evaluation standard is 4.2 %.

The same settings as section 3.2.2 were used for the water system in the practical validation, and the other parameters of the air supply system were set as follows: $t_p = 35$ ℃, $RH_p = 50\%$, $u_p = 2\ m/s$, $t_s = 24$ ℃, $RH_s = 60\%$, $u_s = 2\ m/s$, $s = 4\ mm$, $H = 0.4\ m$, $L = 0.4\ m$. Fig. 11 reflects the simulation results for coverage compared to the experimental results and finds that these points lie within 10% of the deviation and that the maximum difference is 8.2 %, which is acceptable for subsequent studies.

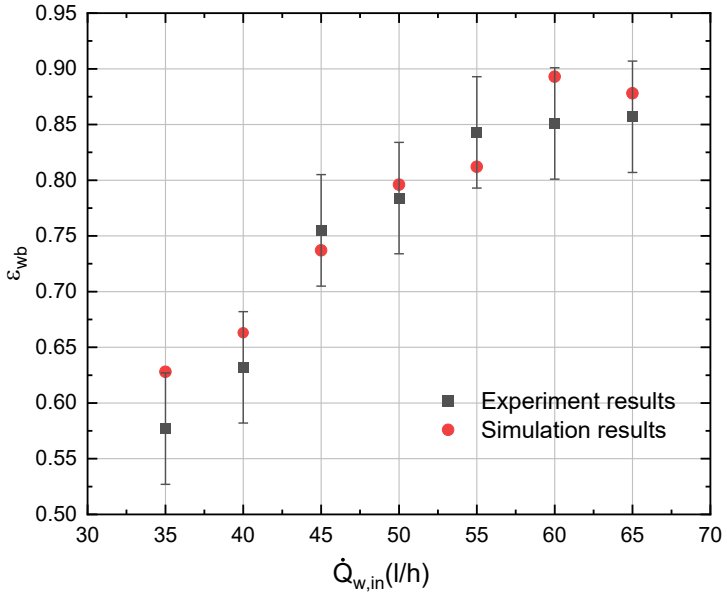


Fig. 11. The model verification results based on wet-bulb efficiency

## 4 Results and discussions

A parametric analysis was carried out unitizing the verified model to identify the effect of parameter variations in the nozzle on the area covered by the water film on the plate surface of the wet channel.

### *4.1 Influence for single nozzle*

#### *4.1.1 Droplet parameter*

In contrast to the other adjustable parameters of the nozzle, the size of the spray droplet was identified as the key influence in this study as a determinant of whether it drifts or not, while the other parameters were maintained steady in the initial simulation step. As demonstrated in Fig. 12 and Fig. 13, the overall water film coverage increased significantly with rising the droplet size at the initial of the diameter expansion, reaching a peak of 0.22 with a diameter of 0.25 mm. Thereafter, as the droplet diameter increased, there was no longer an upward trend and the area covered by the water film instead continued to decrease.

Normally, with a constant flow rate and installation position of the nozzle, if the droplets released from the nozzle are much too small in size with a light weight, they are easily driven by the underside airflow supplied in the wet channel, which results in the droplets being carried away before they arrive into touch with the surface of plate. On the other hand, weight problems can result in droplets with too wide a diameter slipping out of the wetting channel before they arrive in touch with the plate surface. Thus, for the same supply of water rate, an inappropriate droplet size can worsen the area covered by water film, whereas an appropriate size can increase the wetted area up to 61.9%.

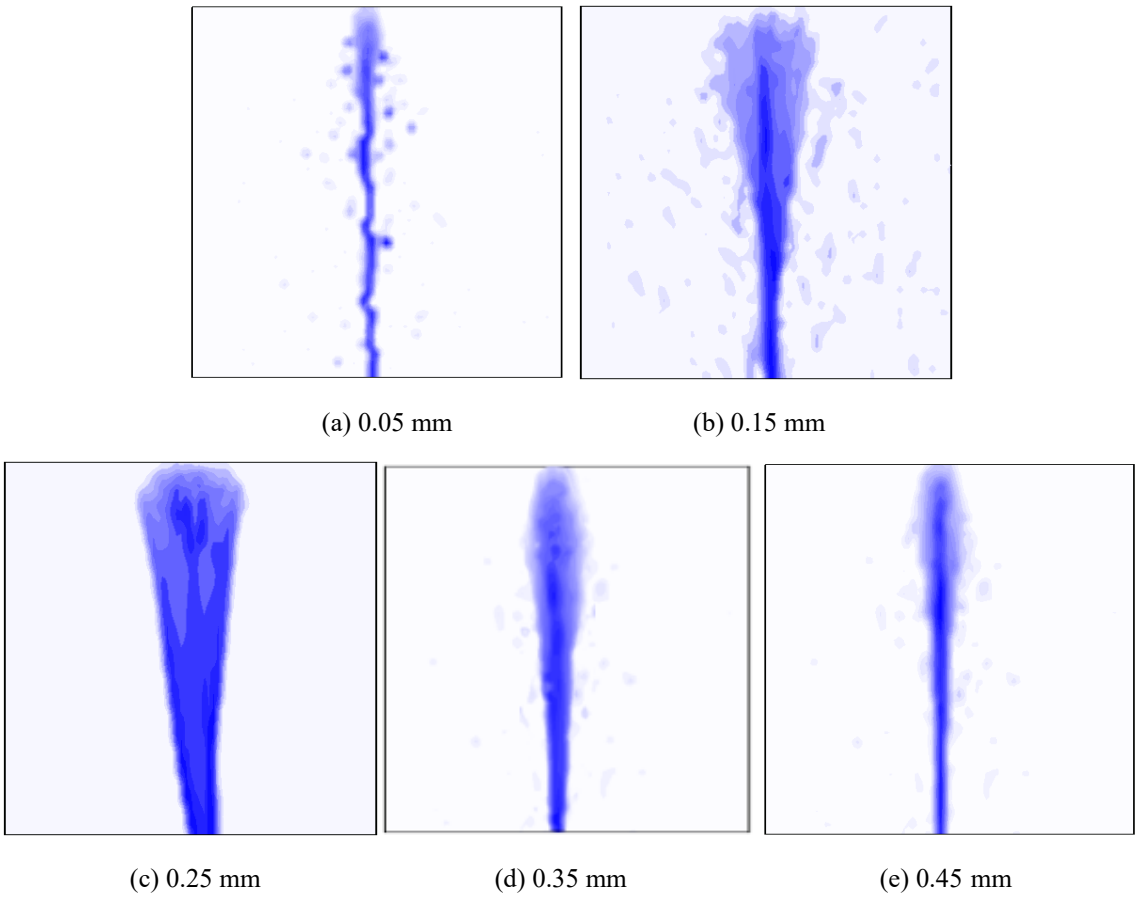

(a) 0.05 mm (b) 0.15 mm

(c) 0.25 mm (d) 0.35 mm (e) 0.45 mm

Fig. 12. Impact of droplet size on the coverage area

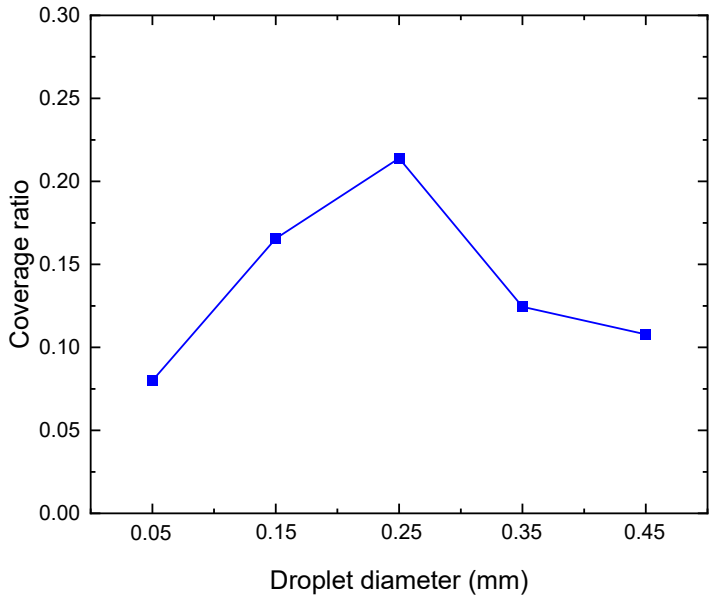


Fig. 13. Trend in the effect of droplet size on the coverage area

*4.1.2 Spray characteristics*

For the purpose of evaluating the effect factor of single nozzle in reality, the fundamental spray characteristics should also be discussed. The actual design notes and prior research have both established the relationships between flow rate, pressure, droplet diameter, and spray cone angle of

nozzles. The following equations represent the primary characteristics nozzles. Lefebvre and McDonell have demonstrated that, the theoretical mass flow rate could be calculated as Eq. (24) [35].

$$\dot{m}_{th} = \rho A_O \left(\frac{2\Delta P}{\rho}\right)^{0.5} \tag{24}$$

The average droplet diameter is obtained from the following equation [35]:

$$d = 9.5 d_j / \left(\Delta P_1 sin(\alpha/2)\right) \tag{25}$$

Besides, the inviscid theory could be seen as the foundation of the correlation for spray cone angle which is formulated as Eq. (26) [36].

$$2\alpha = 334.32 K^{-0.165} \left(\frac{D_S}{D_O}\right)^{-0.484} W_e^{0.043} Re_p^{-0.065} \tag{26}$$

Since the flow rate, pressure, droplet diameter as well as spray cone angle of nozzles are interconnected elements, it is necessary to balance the degree of variations between these factors while maximizing the nozzle performance. Eqs. (24) and (25) demonstrate that the spray flow increases with nozzle spray pressure while the width of the spray droplets decreases. Additionally, the spray cone angle exhibits a tendency of increasing and then dropping when the nozzle pressure and flow rate are raised, which is consistent with the actual design specification. Obviously, the spray droplet diameter is mainly influenced by the jet pressure at the nozzle, and at constant pressure the droplet size is almost constant.

*4.1.3 Spray characteristics determination*

According to the theory and experiments can be proved in a certain range of spray nozzle spray cone angle the larger the better, from angle increases at the same time, the wider the contact range it can spray. In addition, the larger flow rate supply gives the nozzle a denser droplet, which to some extent increases the area covered by the liquid film on the plate. However, due to the linked nature of the variables in the nozzle, it is not possible to avoid the impact on other factors by simply adjusting one factor in isolation. It is therefore essential to maximise the power of the spray in terms of film coverage and to balance the effects of each factor.

The size of the spray droplet diameter will be the primary consideration in this study so as to better control the smooth entry of the droplet into the airflow channel and the smooth contact with the wall. Based on the conclusions of the analysis in section 4.1.2, 0.25 mm should be set as the ideal droplet diameter to be pursued in the study. Besides, three common nozzles with spray diameter of 2.8 mm, 3.0 mm and 3.2 mm were arranged as the main object of this study, and Fig. 14 reflects the parameter characteristics of the three nozzles in order from left to right according to the different pressures at once. With reference to the results demonstrated in Fig. 14, although the droplet diameter (calculated by Eq. (25)) of all three nozzles is close to 0.25 mm at an operating pressure of 1.5 bar, but the spray cone angle of nozzle 1 is too small, while nozzle 3 can reach the maximum spray cone angle but the water consumption is too high. Therefore, the nozzle with a spray diameter of 3.0 mm will be the ideal object of study and its operating condition will be set at a pressure of 1.5 bar, while the spray flow rate is 5.4 l/min and the spray cone angle is 68°.

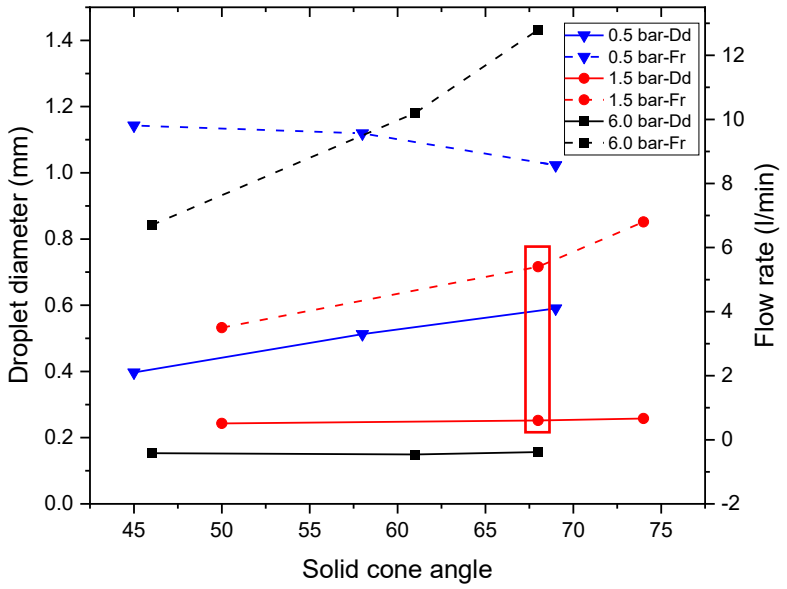


Fig. 14. The characteristics of nozzle spray

*4.1.4* Shrinkage phenomenon

As the material of the heat exchanger is usually aluminium plate, and the spray medium is water with high tension, so as the water film slips, it will inevitably produce the phenomenon of liquid film contraction, making the liquid film away from the secondary airflow outlet the smaller the coverage area [37]. The water droplet membrane consists of the main part of the membrane thickness is basically uniform and there is a raised edge part of the composition. In the direction of flow, the length of the droplet membrane becomes smaller, representing the droplet film gradually shrinks. Thus, in the 3D model, the evaporative heat absorption process within the wet channel takes place only in the wetted area. However, in the 2D model it is unrealistic to assume that evaporation occurs over the entire heat exchanger, as it is not possible to simulate film shrinkage. As a consequence of the contraction of falling film in the direction of flow, it is evident from the 3D simulation that the evaporation process inside the moist channel is not uniform, as shown in Figure 9. However, neither the film contraction nor the non-uniform mass transfer process can be depicted by a two-dimensional simulation, which clearly demonstrates the need for 3D simulations.

*4.2 Influence for multi-nozzles*

As the above discussion is based on a single-pass heat exchanger, whereas the actual IECs are always multi-pass heat exchangers, a simple discussion of the spray distribution placed vertically above the airflow channels is inadequate. This section will focus on the analysis of the heat exchanger channels that can be covered by a film of water when receiving water spray, from close to far apart from the nozzle. As the nozzle height is fixed at 0.15 m and the spray cone angle is 68°, the maximum distance covered by the outgoing spray is 80 mm, but based on practical conditions about 60 mm is already the limit. The progressive interval was therefore set to 20 mm and 0.25 mm was to be used as the defined droplet spray particle diameter. Fig. 15 illustrates the water film formed by the heat exchanger plate surface receiving a fixed single nozzle spray at different locations, and it could be noted that the best wetting situation of the plate surface occurs at a nozzle of 40 mm.

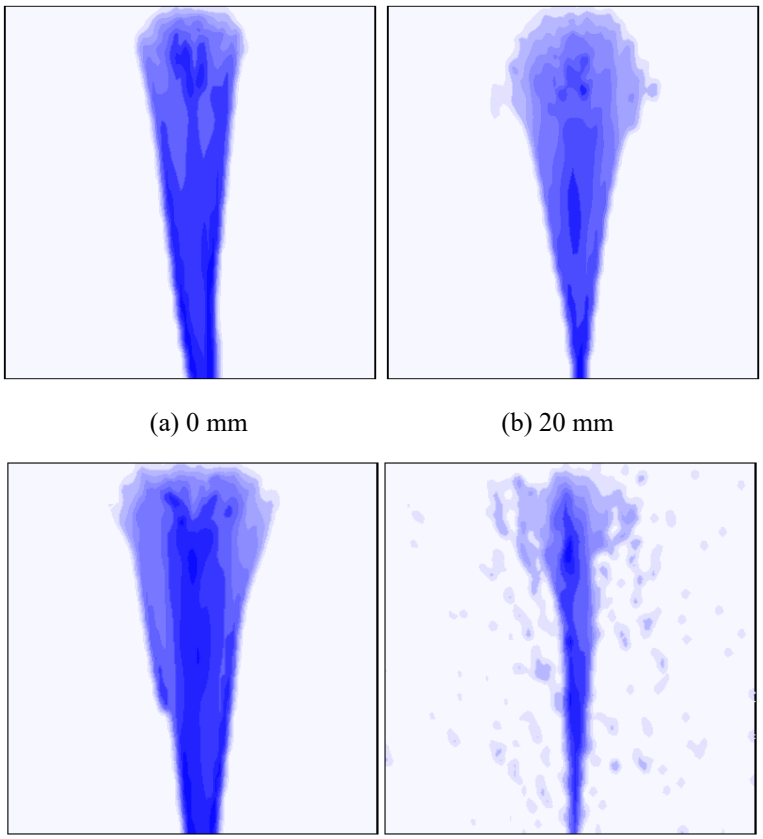

(a) 0 mm (b) 20 mm

(c) 40 mm (d) 60 mm

Fig. 15. Variation of single nozzle to plate distance

In order to determine the optimum spacing of multiple nozzles, the conditions for achieving maximum water film coverage will be evaluated here using two nozzles as an example and the fixed droplet injection particle size of 0.25 mm should be applied. As shown in Fig. 16, once the gap of the two nozzles is extended from 0 mm to 80 mm, the area covered by the water film on the surface of the plate rises from 0.32 to 0.53. Nevertheless, when the nozzle spacing exceeds 80 mm, the area covered by the water membrane reduces dramatically. This occurrence could be attributed to the fact that some droplets escape the boundary when the nozzles are placed too far apart, whereas when they are placed too close together, many droplets collide and splash against one another, preventing the droplets from making contact with the plate and forming a thin film.

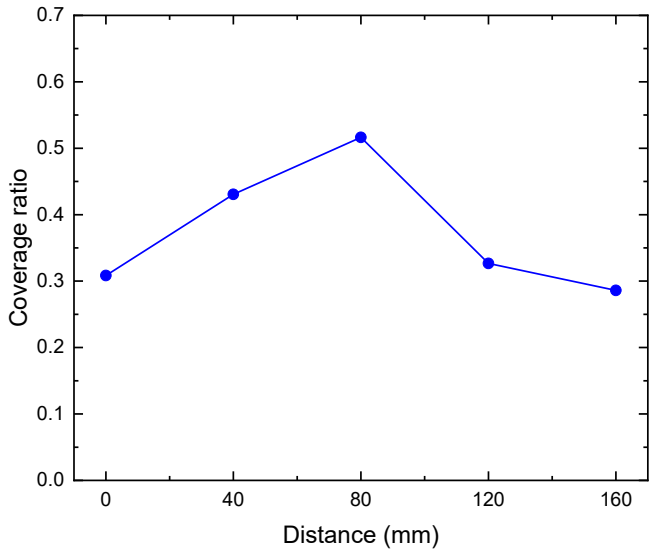


Fig. 16. Impact of distance between two nozzles on coverage factor

*4.3 Influence on IEC performance*

The mathematical model created by Yang et al. [14] was initially utilized here to evaluate the impact of the nozzle settings on the IEC performance. Fig. 17 illustrates how the diameter of droplet generated by the two identical nozzles alters the wet-bulb efficiency. When the wet-bulb efficiency is 52% and the spray droplet size is 0.25 mm, the highest wet-bulb efficiency value is possible. This indicates that simply altering the area coved by the water film on the plate surface while maintaining the corresponding working circumstances, a single parameter, the spray droplet size, may boost wet-bulb efficiency from 35% to 51%.

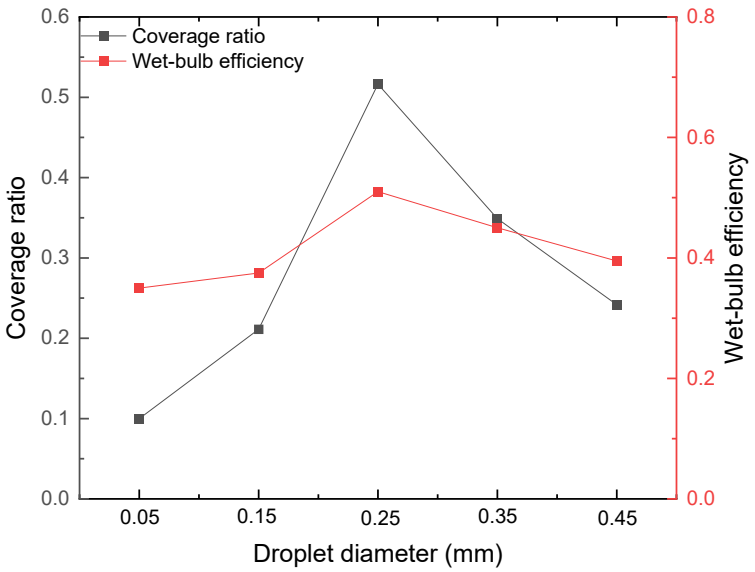


Fig. 17. Impact of droplet size on wet-bulb efficiency

*4.3.1 Optimal arrangement scheme*

Based on the results and analysis in Section 4.1, an optimised nozzle arrangement scheme (Fig. 18(a)) is proposed and a series of performance comparisons of the IEC system are made using the conventional linear arrangement scheme (Fig. 18(b)) and parameter settings investigated experimentally by Antonellis et al. [27] as a reference.

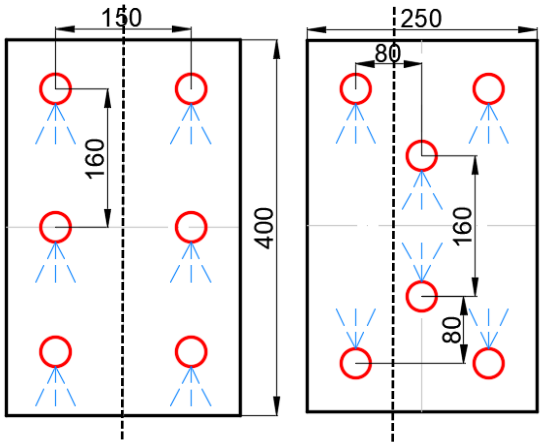


(a) Conventional design (b) Optimized design

Fig. 18. Description of the two comparison arrangement schemes

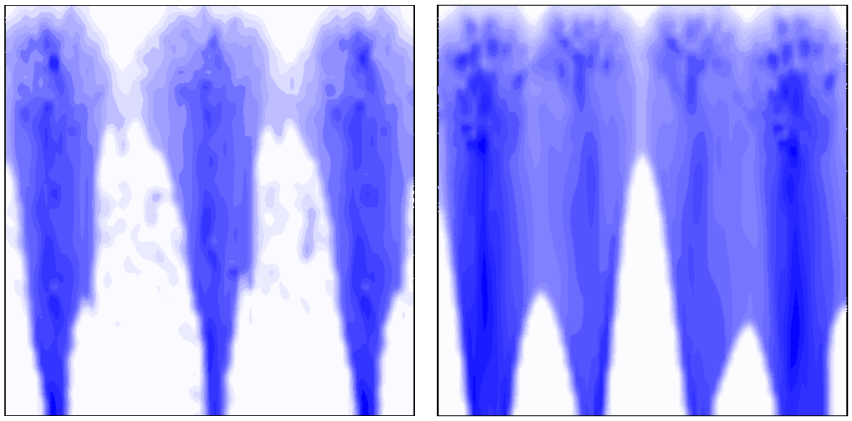

(a) Conventional design (b) Optimized design

Fig. 19. The coverage area situation of the two schemes

Fig. 19 (a) and (b) depict the state of the water film coverage on the plate surface of the heat exchanger furthest from the nozzle (position of the black line in Fig. (18)) for the conventional and optimized schemes, and the water film coverage proportion are 0.72 and 0.91 respectively.

*4.3.2 Temperature distribution*

A case study was carried out at the intake air characteristics and heat exchanger provisions to illustrate the air temperature spread of the IEC before and after the optimization:

$t_p = 35$ ℃, $RH_p = 50\%$, $u_p = 2\ m/s$, $t_s = 24$ ℃, $RH_s = 60\%$, $u_s = 2\ m/s$, $s = 4\ mm$, $H = 0.4\ m$, $L = 0.4\ m$.

The temperature distribution in primary air channel could be seen from Fig. 20. As identified in Fig. 20 (a) and (b), the temperature of the primary airflow drops significantly from the entrance end on the left to the exist end on the right, and the temperature drop is more pronounced close to the exit of the secondary airflow. There are two main reasons for this phenomenon to occur here. Firstly, the air in the upper region of the wet channel is closer to the nozzle and therefore comes into contact with

the spray earlier and more fully, producing a more intense heat mass transfer and resulting in a more dramatic temperature drop. Secondly, as discussed in the previous section, the area covered by the water film in the wetted channel is greatest near the inlet of the secondary air flow and converges as the water film flows downwards, resulting in a contraction of the water film and an inadequate evaporation response compared to the upper part of the channel. Furthermore, a comparison of the temperature spread in the primary channel for nozzle arrangement schemes (a) and (b) confirms that the wider the area covered by the water film, the greater the gradient in temperature reduction, and that lower temperatures can be obtained at the exit of the gas stream when all other parameters are fixed.

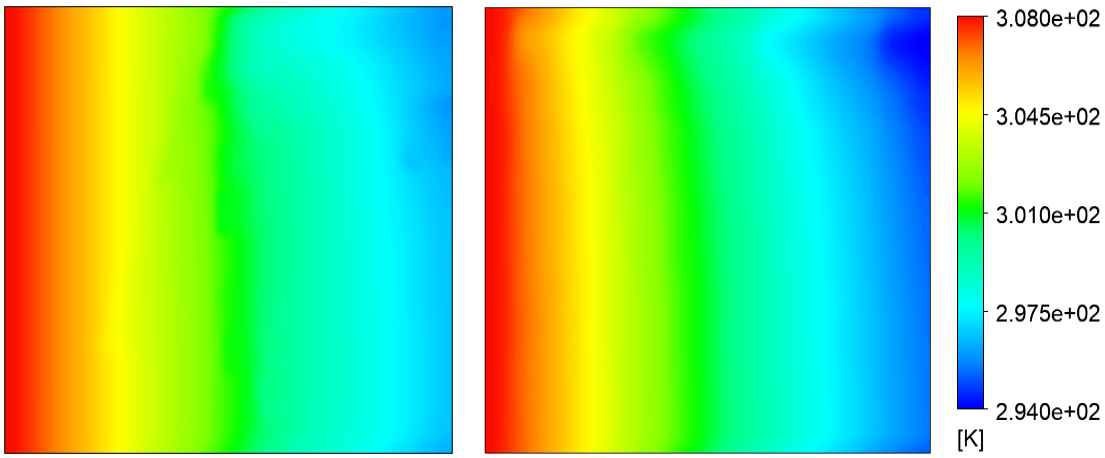


(a) Conventional scheme (b) Optimized scheme

Fig. 20. Temperature distribution of primary air channel

Fig. 21 (a) and (b) describe the fluctuation of wet-bulb efficiency and COP for the IEC with increasing inlet air temperature based on the two different nozzle arrangements, and it can be seen that the overall trend for both is progressively decreasing. However, the wet-bulb efficiency and COP specifications of the optimised IEC system are consistently greater than those of the conventional IEC system, and the improved results are both optimal at an inlet air temperature of 32°C, with increases of 15.1% and 17.6% respectively.

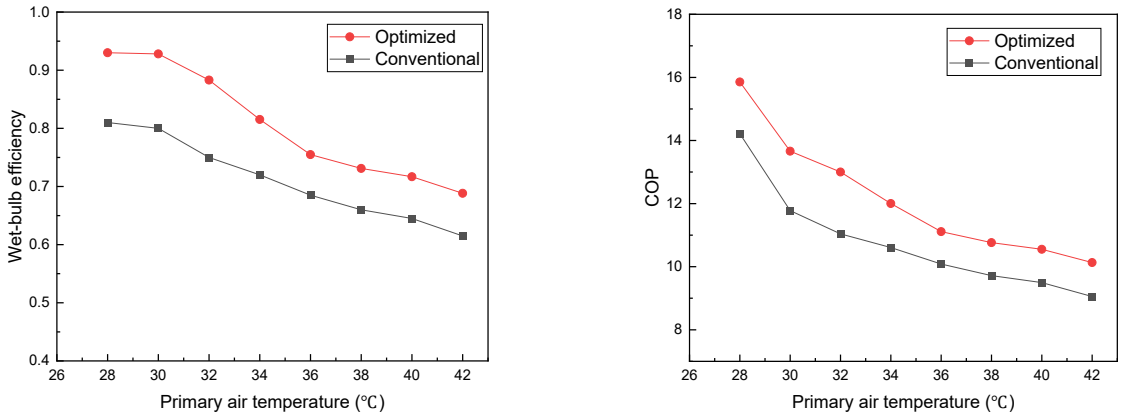


(a) Effect on wet-bulb efficiency (b) Effect on COP

Fig. 21. Effect of inlet primary air temperature on the energy performance of the two IECs

*4.3.4 Velocity of the secondary air*

The influence of the secondary air velocity on the cooling capacity of the IEC with conventional and optimised nozzles is shown in Fig. 22 (a) and (b). It is confirmed that the rise in secondary air velocity reduces the IEC to varying degrees regarding wet-bulb efficiency together with COP. This is because the raise in secondary air mass flow rate reduces both the heat and mass convey between the airflow and the water membrane and with the airflow, as well as the lighter weight spray droplets being blown away. Similarly, the optimised IEC system consistently achieves higher wet-bulb efficiency and COP values than the conventional IEC system, and the improved results are both optimal at an inlet air temperature of 2 m/s, with increases of 10.4% and 14.9% respectively.

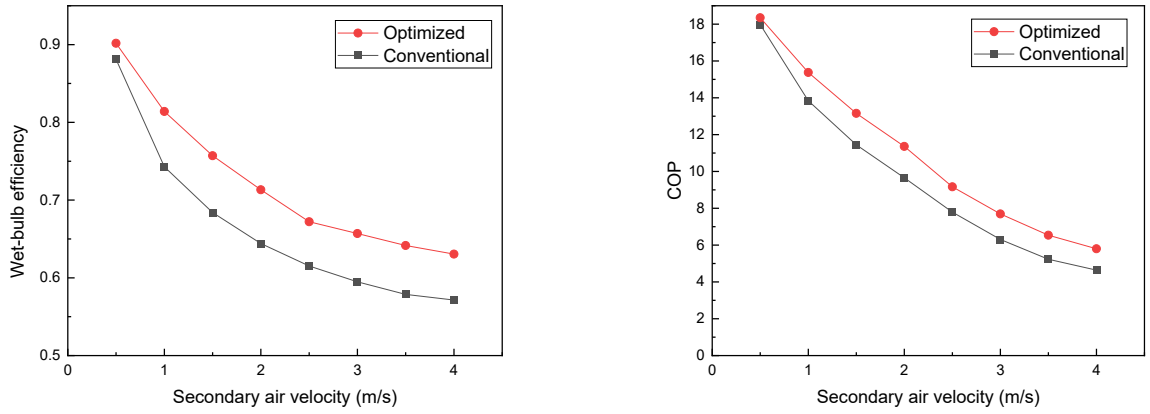


(a) Effect on wet-bulb efficiency (b) Effect on COP

Fig. 22. Effect of secondary air velocity on the energy performance of the two IECs

## 5. Limitations

This paper focuses on the distribution of water membrane within the secondary airflow channels, while the condensation that can occur in dry channels in high humidity areas is not classified for consideration. In addition, the phenomenon of water film shrinkage in the heat exchanger aluminium plate has a substantial effect on the heat transfer process to some extent, and research into more suitable liquid media, hydrophilic materials, is still to be developed.

## 6. Conclusions

In light of the fact that nozzle parameter setting is a crucial impact point in the water membrane coverage area of the IEC exchanger plate surface, this paper firstly proposed and verified a 3D CFD model to consider the actual coverage factor of water film including the cooling performance of the whole IEC system. Then, this paper compares the water film coverage area of wet channel panels with various nozzle parameters and different arrangements. On the basis of the findings, an ideal nozzle design solution is found and contrasted with the traditional one. The final comparison was made between the ideal plan based on the proposed IEC model and the conventional setting of the nozzles in terms of wet-bulb efficiency and COP value of the IEC system. The following are the primary conclusions:

1) The diameter of the spray droplets provided by the water system is an important aspect of the water film on the plate surface. For a single nozzle, a peak membrane coverage ratio of 0.22 could be reached for a spray droplet diameter of 0.25 mm, with an improvement of 61.9% over the worst case scenario.

2) Based on the characteristics of the nozzles, the nozzle parameters for optimum coverage area were set at a droplet diameter of 0.25 mm, a pressure of 1.5 bar, a flow rate of 5.4 l/min and a spray cone angle of 68°.

3) For the presence of multiple nozzles, a spacing of 80 mm was tested and determined to be the optimum arrangement, improving coverage from 0.32 to 0.53 with two nozzles, while increasing IEC system efficiency by 31.4% compared with the worst results.

4) The optimised IEC water distribution system is based on a triangular arrangement of multiple nozzles according to the distance analysis. Compared to conventional settings, the optimised solution provides 20.9% better water film coverage and a significant increase in temperature drop in the primary airflow for the same number of nozzles.

5) For the conventional and optimised nozzle setting scheme, the IEC operating performance follows the same trend with the variation of primary air temperature and secondary air velocity. However, the optimised solution can increase the wet-bulb efficiency and COP by 15.1% and 17.6% respectively under the optimum operating conditions.

## Declaration of Competing Interest

The authors declare that they have no known competing financial interests or personal relationships that could have appeared to influence the work reported in this paper.

## CRediT authorship contribution statement

**Xiaochen Ma:** Conceptualization, Methodology, Experiment, Writing – original draft. **Wenchao Shi:** Validation, Resources, Formal analysis. **Hongxing Yang:** Conceptualization, Supervision, Funding acquisition, Writing – review & editing.

## Acknowledgment

The authors wish to acknowledge the financial support provided by the General Research Fund projects of the Hong Kong Research Grant Council (Ref. No.: 15213219 and 15200420).

## References

[1] Yang H, Shi W, Chen Y, Min Y. Research development of indirect evaporative cooling technology: An updated review. Renew Sustain Energy Rev 2021;145:111082. https://doi.org/10.1016/j.rser.2021.111082.

[2] Shi W, Yang H, Ma X, Liu X. Techno-economic evaluation and environmental benefit of hybrid evaporative cooling system in hot-humid regions. Sustain Cities Soc 2023:104735. https://doi.org/10.1016/j.scs.2023.104735.

[3] International Energy Agency (IEA). The Future of Cooling Opportunities for energy-efficient air conditioning <https://iea.blob.core.windows.net/assets/0bb45525-277f-4c9c-8d0c-9c0cb5e7d525/The_Future_of_Cooling.pdf> 2018:92.

[4] EB. Energy Saving Plan for Hong Kong's Built Environment 2015-2025+ 2015.

[5] Min Y, Chen Y, Shi W, Yang H. Applicability of indirect evaporative cooler for energy recovery in hot and humid areas: Comparison with heat recovery wheel. Appl Energy 2021;287:116607. https://doi.org/10.1016/j.apenergy.2021.116607.

[6] Shi W, Ma X, Gu Y, Min Y, Yang H. Indirect evaporative cooling maps of China: Optimal and quick performance identification based on a data-driven model. Energy Convers Manag 2022;268. https://doi.org/10.1016/j.enconman.2022.116047.

[7] Pérez-Lombard L, Ortiz J, Pout C. A review on buildings energy consumption information. Energy Build 2008;40:394–8. https://doi.org/10.1016/j.enbuild.2007.03.007.

[8] Shi W, Yang H, Ma X, Liu X. A novel indirect evaporative cooler with porous media under dual spraying modes: A comparative analysis from energy, exergy, and environmental perspectives. J Build Eng 2023;76:106874. https://doi.org/10.1016/j.jobe.2023.106874.

[9] Rampazzo M, Lionello M, Beghi A, Sisti E, Cecchinato L. A static moving boundary modelling approach for simulation of indirect evaporative free cooling systems. Appl Energy 2019;250:1719–28. https://doi.org/10.1016/j.apenergy.2019.04.087.

[10] Zhang Y, Zhang H, Yang H, Chen Y, Leung CW. Response surface modeling and optimization scheme of an internally cooled liquid desiccant air conditioning system. J Build Eng 2023;76:107371. https://doi.org/10.1016/j.jobe.2023.107371.

[11] Xuan YM, Xiao F, Niu XF, Huang X, Wang SW. Research and application of evaporative cooling in China: A review (I) - Research. Renew Sustain Energy Rev 2012;16:3535–46. https://doi.org/10.1016/j.rser.2012.01.052.

[12] Min Y, Chen Y, Yang H. A statistical modeling approach on the performance prediction of indirect evaporative cooling energy recovery systems. Appl Energy 2019;255:113832. https://doi.org/10.1016/j.apenergy.2019.113832.

[13] Chen Y, Yang H, Luo Y. Parameter sensitivity analysis and configuration optimization of indirect evaporative cooler (IEC) considering condensation. Appl Energy 2017;194:440–53. https://doi.org/10.1016/j.apenergy.2016.06.121.

[14] De Antonellis S, Cignatta L, Facchini C, Liberati P. Effect of heat exchanger plates geometry on performance of an indirect evaporative cooling system. Appl Therm Eng 2020;173:115200. https://doi.org/10.1016/j.applthermaleng.2020.115200.

[15] Guilizzoni M, Milani S, Liberati P, De Antonellis S. Effect of plates coating on performance of an indirect evaporative cooling system. Int J Refrig 2019;104:367–75. https://doi.org/10.1016/j.ijrefrig.2019.05.029.

[16] You Y, Wang G, Yang B, Guo C, Ma Y, Cheng B. Study on heat transfer characteristics of indirect evaporative cooling system based on secondary side hydrophilic. Energy Build 2022;257:111704. https://doi.org/10.1016/j.enbuild.2021.111704.

[17] Chen Y, Huang X, Sun T, Chu J. Experimental study of plant fiber-polymer composite for indirect evaporative cooler application. Appl Therm Eng 2021;199:117543. https://doi.org/10.1016/j.applthermaleng.2021.117543.

[18] Shi W, Min Y, Ma X, Chen Y, Yang H. Dynamic performance evaluation of porous indirect evaporative cooling system with intermittent spraying strategies. Appl Energy 2022;311:118598. https://doi.org/10.1016/j.apenergy.2022.118598.

[19] Shi W, Min Y, Ma X, Chen Y, Yang H. Performance evaluation of a novel plate-type porous indirect evaporative cooling system: An experimental study. J Build Eng 2022;48:103898. https://doi.org/10.1016/j.jobe.2021.103898.

[20] Sun T, Huang X, Chen Y, Zhang H. Experimental investigation of water spraying in an indirect evaporative cooler from nozzle type and spray strategy perspectives. Energy Build 2020;214:109871. https://doi.org/10.1016/j.enbuild.2020.109871.

[21] De Antonellis S, Joppolo CM, Liberati P, Milani S, Romano F. Modeling and experimental study of an indirect evaporative cooler. Energy Build 2017;142:147–57. https://doi.org/10.1016/j.enbuild.2017.02.057.

[22] Sotelo-Salas C, Pozo CE del, Esparza-López CJ. Thermal assessment of spray evaporative cooling in opaque double skin facade for cooling load reduction in hot arid climate. J Build Eng 2021;38. https://doi.org/10.1016/j.jobe.2021.102156.

[23] Ma X, Shi W, Yang H. Study on water spraying distribution to improve the energy recovery performance of indirect evaporative coolers with nozzle arrangement optimization ☆. Appl Energy 2022;318:119212. https://doi.org/10.1016/j.apenergy.2022.119212.

[24] C. Kettleborough CH. The thermal performance of the wet surface plastic plate heat exchanger used as an indirect evaporative cooler 1983.

[25] Ren C, Yang H. An analytical model for the heat and mass transfer processes in indirect evaporative cooling with parallel/counter flow configurations. Int J Heat Mass Transf 2006;49:617–27. https://doi.org/10.1016/j.ijheatmasstransfer.2005.08.019.

[26] Cui X, Chua KJ, Islam MR, Ng KC. Performance evaluation of an indirect pre-cooling evaporative heat exchanger operating in hot and humid climate. Energy Convers Manag 2015;102:140–50. https://doi.org/10.1016/j.enconman.2015.02.025.

[27] De Antonellis S, Joppolo CM, Liberati P. Performance measurement of a cross-flow indirect evaporative cooler: Effect of water nozzles and airflows arrangement. Energy Build 2019;184:114–21. https://doi.org/10.1016/j.enbuild.2018.11.049.

[28] Yang M, Ma H, Ma S, Nong A, Zhang Y, Ma Y. Effect of surface wettability on air parameters and performance of indirect evaporative cooler in the presence of primary air condensation. J Build Eng 2022;45:103535. https://doi.org/10.1016/j.jobe.2021.103535.

[29] Yu J, Jin S, Xia Y. Experimental and CFD investigation of the counter-flow spray concentration tower in solar energy air evaporating separation saline wastewater treatment system. Int J Heat Mass Transf 2019;144:118621. https://doi.org/10.1016/j.ijheatmasstransfer.2019.118621.

[30] Sadighi Dizaji H, Hu EJ, Chen L, Pourhedayat S. Analytical/experimental sensitivity study of key design and operational parameters of perforated Maisotsenko cooler based on novel wet-surface theory. Appl Energy 2020;262:114557. https://doi.org/10.1016/j.apenergy.2020.114557.

[31] Min Y, Chen Y, Yang H. Numerical study on indirect evaporative coolers considering condensation: A thorough comparison between cross flow and counter flow. Int J Heat Mass Transf 2019;131:472–86. https://doi.org/10.1016/j.ijheatmasstransfer.2018.11.082.

[32] Kong XQ, Wang RZ, Huang XH. Energy efficiency and economic feasibility of CCHP driven by stirling engine. Energy Convers Manag 2004;45:1433–42. https://doi.org/10.1016/j.enconman.2003.09.009.

[33] Ma X, Shi W, Yang H. Improving the performance of indirect evaporative cooler for energy recovery from the perspective of nozzle configuration: A CFD model analysis. J Build Eng 2023;76:107195. https://doi.org/10.1016/j.jobe.2023.107195.

[34] Wang Q, Yao Y, Shen Z, Yang H. A hybrid parabolic trough solar collector system integrated with photovoltaics. Appl Energy 2023;329:120336. https://doi.org/10.1016/j.apenergy.2022.120336.

[35] Jain M, John B, Iyer KN, Prabhu S V. Characterization of the full cone pressure swirl spray nozzles for the nuclear reactor containment spray system. Nucl Eng Des 2014;273:131–42. https://doi.org/10.1016/j.nucengdes.2014.02.025.

[36] Lan Z, Zhu D, Tian W, Su G, Qiu S. Experimental study on spray characteristics of pressure-swirl nozzles in pressurizer. Ann Nucl Energy 2014;63:215–27. https://doi.org/10.1016/j.anucene.2013.07.048.

[37] Tao W, Yimo L, Lin L. A novel 3D simulation model for investigating liquid desiccant dehumidification performance based on CFD technology. Appl Energy 2019;240:486–98. https://doi.org/10.1016/j.apenergy.2019.02.068.